A LARGE TRAINING DATASET OF BOULDER SIZES AND SHAPES AS A FIRST STEP TOWARDS THE AUTOMATED DETECTION OF ROCK FRAGMENTS ON PLANETARY SURFACES. N.C. Prieur[1,2], L. Rubanenko[1], Z. Xiao[3], H. Kerner[4], S.C. Werner[2] and M.G.A. Lapôtre[1], [1]Stanford University, Stanford, CA, USA (nilscp@stanford.edu). [2]Department of Geosciences, University of Oslo, Norway. [3]Sun Yat-Sen University, Zhuhai, China. [4]University of Maryland, College Park, MD, USA.

Introduction: Boulders – here defined as rock fragments resolvable in high-resolution orbital imagery – abound on planetary surfaces, and form through a variety of geological processes. Notably, rock fragments are ejected upon meteor impact and deposited elsewhere on the surface, where they sometimes form secondary craters. By increasing the density of impact craters, secondary impacts distort crater statistics, and in doing so, bias estimated surface ages. As the only directly measurable and quantifiable portion of ejected materials (Fig. 1), impact-generated boulders offer a unique opportunity to constrain the size and velocity distribution of ejected rock fragments, and thus, to correct for any biases in planetary surface age determinations [1].

As hundreds of thousands of detectable boulders are often associated with a single impact structure [2–4], manual mapping of individual boulders is a laborious and time-consuming task. Thus, automating the boulder-detection process will be critical in the acquisition of high-quality and significant boulder statistics over large and varied planetary surfaces. Three main boulder-detection algorithms have been developed to date [5–7].

Two of these algorithms utilize the shadows cast by boulders to detect boulders [5–6]. Specifically, Golombek et al. (2008) [5] apply a segmentation technique to extract contours of boulder shadows. An ellipse is then fitted through each shadow outline to infer both boulder height and width. Li and Wu (2018) [6], conversely, developed a detection routine that relies on brightness contrasts along the illumination direction, using abrupt changes from bright to dark pixels as a detection proxy. Both algorithms have been tested over several locations on the Moon [6] and Mars [5,8–9]. Such tests involve the comparison of automated measurements of boulders and corresponding cumulative fractions of surface coverage for boulders of specific diameters (plotted in logarithmic space) with manually derived ones – an approach that tends to inherently minimize potential differences between both datasets – or through comparisons of measured and predicted surface areas covered by boulders, which, without groundtruthed data, does not permit to evaluate performance (accuracy, precision, recall). Furthermore, the presence of primary and secondary impact craters casting shadows in our regions of interest would present a significant challenge to shadow-based boulder-detection algorithms. Because Golombek et al. (2008) [5] were most concerned with landing-site characterization, which are highly skewed towards flat terrains, topographic roughness was not a major concern for their detection algorithm. Although the method of Li and Wu (2018) [6] may permit to discern boulders from other shadow-casting landforms, it is still expected to yield a significant number of false detections in rough terrains, as brightness contrasts along crater rims resemble those surrounding boulders.

Finally, Bickel et al. (2019) [7] made use of a Convolutional Neural Network (CNN) to automatically detect rockfalls. CNNs are powerful deep supervised learning models that use images of an object of interest as input to automatically classify similar objects in a new set of images [10–12]. Specifically, Bickel et al. (2019) [7] trained the RetinaNet CNN object detection model to generate a global map of rockfalls of the lunar surface [13]. However, because they were focused on the mapping of rockfalls, their detection algorithm relies on the presence of boulder tracks and was not trained to detect boulders that are not associated with boulder tracks.

Our goal is to develop and train a versatile boulder-detection algorithm using the instance segmentation Mask R-CNN model architecture [14] that enables the characterization of boulder size and shape distributions on planetary surfaces.

Methods and Preliminary Results: Detection of boulders using Mask R-CNN requires training of the algorithm with a comprehensive dataset. To circumvent some of the issues encountered by rule-based detection algorithms and detect boulders reliably in a multitude of surface conditions, it is important for the training dataset to include images with different illumination conditions, boulder sizes, and density. As a first step towards training the Mask R-CNN model to detect boulders on planetary surfaces, we acquired a large training dataset of boulder sizes and shapes from high-resolution, Lunar Reconnaissance Orbiter Camera (LROC) Narrow Angle Camera (NAC) [15] images (~0.50 m/pixel) of the 3.8 km Censorinus impact crater (0.4°S, 32.7°E, Fig. 1). Censorinus is one of the freshest impact craters on the lunar surface, making it an ideal first target.

Manually mapping boulders from orbital imagery present several challenges. Whereas the identification

of large boulders located near crater rims is relatively trivial (Fig. 2a), the bulk of boulders have sizes close to the resolution limit (Fig. 2b). The size of boulders decreases abruptly away from the crater rim (Fig. 2b) [4] as is expected from extensive fragmentation of ejected materials upon impact and lower ejection velocities for larger fragments. As fragmented boulders typically reflect considerably more light than background regolith (Fig. 2c), they often cause an oversaturation of pixels, and the blurring of neighboring pixels, yielding poorly defined boulder contours (Fig. 2d). In such conditions, and near the resolution limit, the distinction of single boulders from multiple tightly-spaced boulders is challenging. In addition, significant variations in the degree of boulder burial are observed across the rim and within the crater (Fig. 2e,f). Therefore, depending on the degree of burial, fragmentation state, and brightness contrast, even a 20x20 pixels boulder could be challenging to characterize accurately in some instances (Fig. 2e,f).

With these constraints in mind, we focused on boulders defined as any rock fragment larger than 5 pixels in width or length, regardless of its degree of burial. We traced the exact outline of 6,000 boulder labels (as of January 2022) using the QGIS software. To date, we focused on NAC images with solar incidence angle between 0–40° to minimize shadows.

Future Work: In upcoming months, we will continue gathering training data around impact craters on the Moon, Mars, and asteroids to build a versatile training dataset for Mask R-CNN to detect boulders automatically on planetary surfaces. At the conference, we will present all data acquired to date and a preliminary analysis of the spatial distribution of boulder sizes and shapes around impact craters on multiple planetary bodies.

Acknowledgments: NCP acknowledges support from the European Commission (101030364) and Research Council of Norway (328597) through the MSCA-2020 Individual Global Fellowship hosted at Stanford University and the University of Oslo.

References: [1] Melosh (1984) Icarus 59. [2] Krishna et al. (2016) Icarus 264. [3] Pajola et al. (2019) PSS 165. [4] Watkins et al. (2019) JGR Planets 124. [5] Golombek et al. (2008) JGR Planets 113. [6] Li & Wu. (2018) JGR Planets 123. [7] Bickel et al. (2019) IEEE Geo and R. Sensing 57. [8] Golombek et al. (2012) Mars 7. [9] Golombek et al. (2017) Space Sc. Rev. 211. [10] LeCun et al. (1989) Neural Comp. 1. [11] DeLatte et al (2019) Advances in Space Res 64. [12] Kerner et al. (2019) IEEE J. App. Earth Obs. and R. Sensing 12. [13] Bickel et al. (2020) Nature Comm 11. [14] He et al. (2017) arXiv. [15] Robinson et al. (2010) Space Sc. Rev. 150.

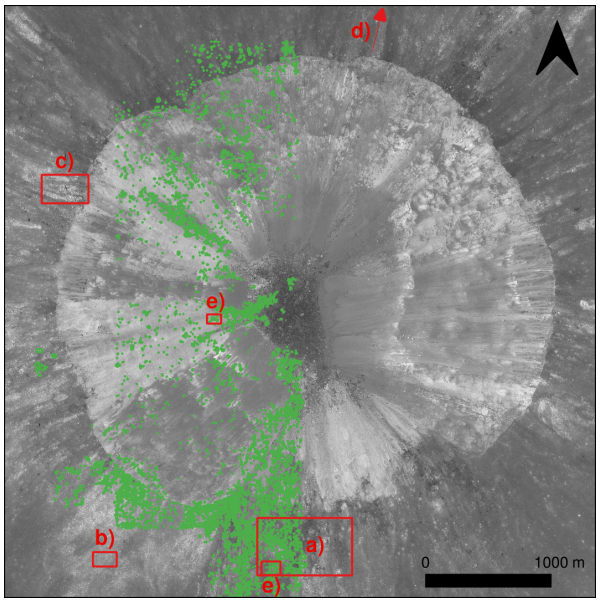

Fig. 1 (a) LROC NAC images of Censorinus crater on the Moon, with boulders labeled to date (green). Red boxes outline locations of panels in Fig 2 (a–f).

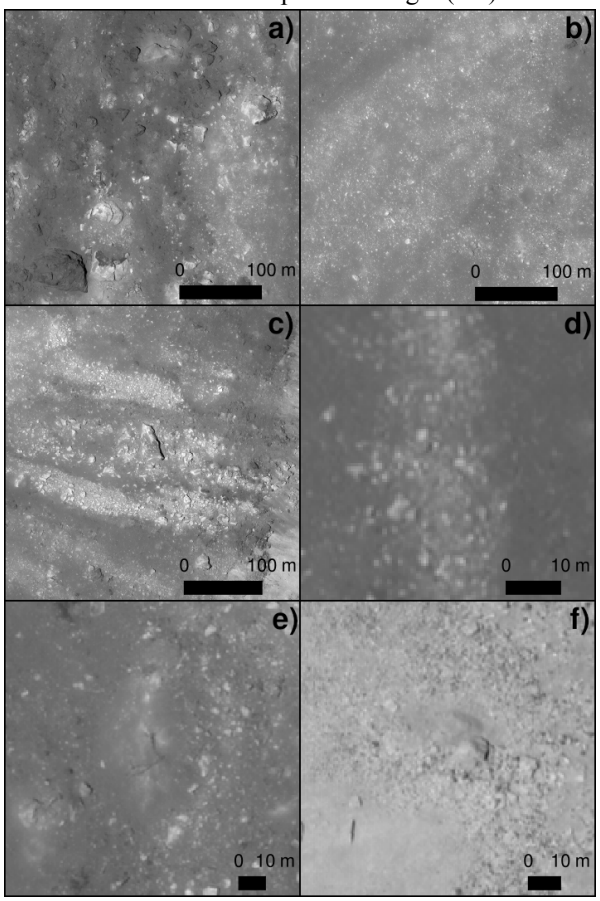

Fig. 2 (a) Large boulders located near the Censorinus crater rim. (b) Field of small boulders with diameters near the image resolution limit. (c,d) Fragmented boulders. (e,f) Partially buried boulders.